



Subtractive synthesis of anatase TiO₂ nanostructures for sustained Li-storage in faradaic and non-faradaic assemblies

Shaji Jyothilakshmi^a, Yun-Sung Lee^{b,*}, Vanchiappan Aravindan^{a,**}

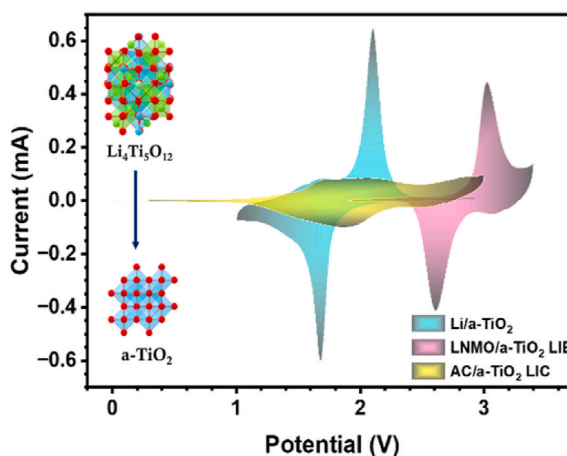
^a Department of Chemistry, Indian Institute of Science Education and Research (IISER), Tirupati, 517619, India

^b School of Chemical Engineering, Chonnam National University, Gwang-ju, 61186, Republic of Korea

HIGHLIGHTS

- We report the successful subtractive synthesis of TiO₂ from Li₄Ti₅O₁₂ anode.
- A high-energy Li-ion battery (LIB) is fabricated with LiNi_{0.5}Mn_{1.5}O₄ cathode.
- High-power Li-ion Capacitor (LIC) is fabricated with an activated carbon cathode.
- LIB and LIC delivered the maximum energy densities of 188 and 73 Wh kg⁻¹.

GRAPHICAL ABSTRACT



ARTICLE INFO

Keywords:

Reverse synthesis
Anatase TiO₂
Li-ion battery
Li-ion capacitor
Recycling

ABSTRACT

Titanium dioxide has been considered one of the promising anode materials for energy storage applications since the 1980s, especially in lithium-ion batteries (LIBs). Among the different polymorphs, the anatase phase of titanium dioxide (a-TiO₂) exhibits an excellent composition of physical and chemical properties with high capacity, superior rate capability, and cyclability. Herein, we report a method of reverse synthesizing TiO₂ through the leaching of lithium titanate (Li₄Ti₅O₁₂, LTO). The physical and chemical properties of the synthesized a-TiO₂ were examined through various characterization techniques, and its formation was confirmed. Initially, the electrochemical Li-storage ability of the a-TiO₂ was analyzed through Li/a-TiO₂ half-cell assembly. Further, LIB and lithium-ion capacitors (LICs) were fabricated by pairing a-TiO₂ with LiNi_{0.5}Mn_{1.5}O₄ (LNMO) and activated carbon (AC), respectively. A maximum energy and power density of 188 and 73 Wh kg⁻¹ was shown by LNMO/a-TiO₂ (LIB) and AC/a-TiO₂ (LIC) assemblies, respectively. Both the LIB and LIC exhibited good cyclability and excellent adaptability at various temperatures.

* Corresponding author

** Corresponding author.

E-mail addresses: aravind.van@gmail.com, aravind_van@yahoo.com (V. Aravindan).

<https://doi.org/10.1016/j.jpowsour.2025.237543>

Received 15 February 2025; Received in revised form 19 April 2025; Accepted 1 June 2025

Available online 14 June 2025

0378-7753/© 2025 Elsevier B.V. All rights are reserved, including those for text and data mining, AI training, and similar technologies.

1. Introduction

High-power hybrid capacitors and high-energy batteries are revolutionizing the field of energy storage, which significantly raises the demand for electric vehicles and the utilization of clean energy to reduce carbon footprints. Lithium-ion capacitors (LICs) and lithium-ion batteries (LIBs) are the most popular systems of choice, offering high power density ($>10 \text{ kW kg}^{-1}$) and high energy density ($150\text{--}300 \text{ Wh kg}^{-1}$), respectively [1,2]. The energy storage capability of the LIC and LIB is largely determined by suitable redox active materials as the anodes. Even though graphite is the most successful commercial anode, it suffers safety concerns due to dendrite formation at higher rates and the solid-electrolyte interface (SEI), which results in exothermic reactions and irreversible capacity loss [3]. Therefore, many other anode materials, such as transition metal oxides, Sn-based, and Si-based materials, have attracted the attention of researchers. In this line, titanium dioxide (TiO_2) polymorphs as anode materials for energy storage were reported in 1980 [4,5]. Especially the anatase phase of TiO_2 has excellent physical and chemical properties like high theoretical capacity (335 mAh g^{-1}), reasonable reduction potential ($\sim 1.75 \text{ V vs. Li}$) higher than graphite that helps to charge at high rates with improved safety, $<4\%$ of volume expansion, negligible dendrite, and no SEI formation [5–8]. This is because the de/insertion potential falls within the thermodynamic stability window of 0.8 V vs. Li of the conventional carbonate-based electrolyte [1]. In addition, TiO_2 is a non-toxic, low-cost, environmentally friendly anode material. However, developing a simple synthesis strategy for TiO_2 over complex, time-consuming reactions is very challenging [9].

Within this context, we herein report a simple, scalable mechanical and chemical method to synthesize TiO_2 from commercial lithium-titanate ($\text{Li}_4\text{Ti}_5\text{O}_{12}$, LTO). This study has attempted to establish the reutilization protocol to foresee the accumulation of the large amount of LTO-based LIBs discarded from electric vehicles and stationary applications for recycling. Here, we have leached out anatase phase TiO_2 (a- TiO_2) from LTO using HCl and further thermally treated at a temperature of 400°C . The formation, structure, and morphology of a- TiO_2 were confirmed through various analytical and characterization techniques. Then, the potential of the synthesized a- TiO_2 as an anode for Li-storage was analyzed by fabricating a LIB with $\text{LiNi}_{0.5}\text{Mn}_{1.5}\text{O}_4$ (LNMO) cathode and with activated carbon (AC) for LIC assembly. Prior to the full-cell assembly, the individual electrochemical performance of all the electrodes (anode and cathodes) was studied in a half-cell assembly vs. Li, and their mass loading was adjusted according to the half-cell performance. Intense physicochemical and electrochemical studies were conducted and are further discussed in detail in the upcoming sections.

2. Experimental section

Synthesis of bulk TiO_2 :

Bulk TiO_2 was prepared from commercially available Lithium titanate ($\text{Li}_4\text{Ti}_5\text{O}_{12}$ – LTO). LTO was subjected to high-energy mechanical milling (HEMM) for 30 min. Around 0.5 g of this ball-milled LTO was taken, and 30 mL of 1 M HCl was added to it under constant stirring at 450 rpm at room temperature overnight. The resultant was centrifuged

and washed with deionized water until the pH became neutral. The residue was kept for drying overnight at room temperature. The intermediate product was calcined in a box furnace (Carbolite, UK) in an air atmosphere for 5 h at 400°C to obtain a- TiO_2 , as shown in Scheme 1. The activated carbon (AC) and $\text{LiNi}_{0.5}\text{Mn}_{1.5}\text{O}_4$ (LNMO) had been purchased commercially (MTI, USA) and used directly without any further purification.

2.1. Material characterization

Rigaku Smartlab automated multipurpose X-ray diffractometer was used to examine the crystallographic nature and phase of a- TiO_2 with a monochromatic $\text{Cu K}\alpha$ radiation ($\lambda = 1.5604 \text{ \AA}$) in a scan rate of 2° min^{-1} . The surface elemental composition and oxidation states of Titanium and Oxygen in a- TiO_2 were analyzed through high-resolution X-ray photoelectron spectroscopy (XPS) multi-lab instrument with a monochromatic $\text{Al K}\alpha$ radiation $h\nu = 1486.6 \text{ eV}$, 2000, UK. The structural morphology, size, and characteristics of a- TiO_2 were studied using a field emission scanning electron microscope (FE-SEM), Zeiss Gemini 560, Germany, and a high-resolution transmission electron microscopy (HR-TEM), JEM-2000, EX-II, JEOL, Japan. An automated gas sorption analyzer, Autosorb IQ-XR-XR, 3 stat, Viton for Brunauer-Emmett-Teller (BET) measurements, was used to determine the physical properties of a- TiO_2 . The surface elemental composition of a- TiO_2 was identified with the help of energy-dispersive X-ray spectroscopy (EDS).

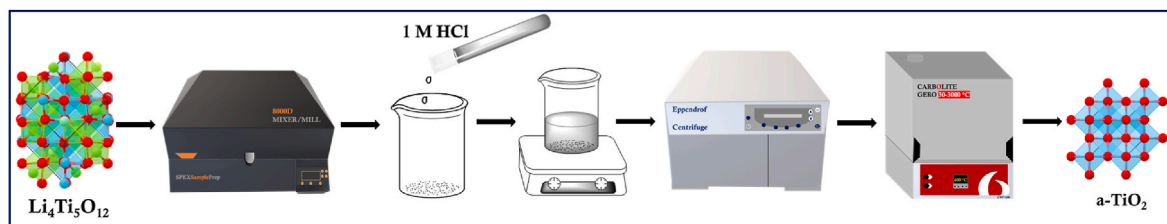
2.2. Electrochemical characterization

2.2.1. Electrode fabrication

The a- TiO_2 , $\text{LiNi}_{0.5}\text{Mn}_{1.5}\text{O}_4$ (LNMO), and Activated carbon (AC) electrodes were prepared manually by mortar and pestle. 10 mg of active material (a- TiO_2 & LNMO), 2 mg of acetylene black (AB) (conductive carbon), and 2 mg of teflonized acetylene black (TAB-2, binder) were mixed together in a ratio of $10:2:2$ with ethanol as a solvent medium until a free-standing thin film is obtained. The film was pressed onto a stainless-steel mesh (SS, Nominal aperture: 0.38 mm , Goodfellow, UK) of 14 mm diameter using a hydraulic press (Specac, UK) with an average mass loading of 6.5 mg cm^{-2} . The AC electrodes were prepared at an $8:1:1$ ratio with a mass loading of 5.2 mg cm^{-2} . Similarly, the LNMO and AC electrodes for full cell performance studies of LIB and LIC, respectively, were prepared by the active material loading adjusted to balance the capacity of the anode. The ratio of a- TiO_2 : LNMO and a- TiO_2 :AC were fixed to $1:1.4$ (2.5 mg : 3.5 mg) and $1:3$ (2.5 mg : 7.5 mg), respectively. The anode a- TiO_2 was electrochemically pretreated before full-cell assembly to avoid any capacity fading or irreversibility issue caused by the anode in the LIB/LIC.

2.3. Half-cell and full-cell fabrication

The electrodes were kept overnight in a vacuum oven at 75°C for proper drying and complete moisture removal from the electrode surface before coin-cell fabrication. The a- TiO_2 , LNMO, and AC half cells were fabricated using lithium as the reference and counter electrode for electrochemical studies. 1 M LiPF_6 in ethylene carbonate (EC) and



Scheme 1. The simple representation showing the synthesis of a- TiO_2 .

dimethyl carbonate (DMC) (LiPF_6 , LIPASTE, Tomiyama) in a 1:1 v/v ratio was used as the electrolyte, and a glass microfiber filter paper (Whatman, cat no. 1825-047, UK) as the separator. The LIB and LIC were fabricated using a-TiO₂ as the anode and LNMO and AC as the cathode, respectively, under a balanced mass loading condition. Both the half and full cells have been assembled in an argon-filled glove box workstation (MBraun, Germany) under a maintained condition of O₂ < 0.1 ppm and H₂O < 0.1 ppm in a CR2016 coin cell. The BioLogic battery tester (BCS-805) was used to evaluate the electrochemical performance of the fabricated half-cells and full-cells, and an Espec SU-242 benchtop-type environmental chamber was used to perform temperature-dependent studies of the cells. All the half cells exhibited an open circuit voltage (OCV) of ~3 V vs. Li.

3. Result and discussion

Fig. 1a shows the X-ray diffraction (XRD) pattern of powdered a-TiO₂ synthesized by leaching of LTO exhibits pure phase structure without any traces of impurity. The sharp and well-defined peaks indicate the high crystallinity of the sample. The XRD pattern of a-TiO₂ belongs to the standard anatase TiO₂ of JCPDS card No. 21-1272. The prominent peaks (2 θ) of a-TiO₂ at ~25.2, 37.7, 47.8, 53.7, 54.8, 62.5, 68.6, 70.2, and 74.9 represent the (101), (004), (200), (105), (211), (204), (116), (220), and (215) crystal lattice planes, respectively. The synthesized a-TiO₂ belongs to the $I4_1/amd$ space group with a tetragonal structure. The phase is composed of two TiO₆ octahedra, sharing the corners with two other TiO₆ octahedra [4,10]. The unit cell parameters are $a = b = 3.7852 \text{ \AA}$, $c = 9.5139 \text{ \AA}$, $\alpha = \beta = \gamma = 90^\circ$. The particle size of the a-TiO₂ was calculated and obtained as 14 nm using the Debye-Scherrer equation [11] as follows:

$$D = K\lambda / \beta \cos \theta$$

Where $K = 0.9$ is the constant, $\lambda = 0.154 \text{ nm}$ is the X-ray source

wavelength, β is the full width at half maximum of the peaks in radians, and θ is the Bragg's angle in radians.

The surface elemental composition of the a-TiO₂ has been studied using X-ray photoelectron spectroscopy (XPS). To determine the chemical/oxidation states, deconvolution of the Ti 2p and O 1s has been done for the individual elements (Fig. 1b and c). The spectra of Ti 2p exhibit two pairs of peaks at ~462.2 and ~456.5 eV corresponding to the Ti 2p_{1/2} and Ti 2p_{3/2} states, indicating that the Ti in the a-TiO₂ is in the Ti⁴⁺ oxidation state [12]. The deconvolution of O 1s core level produces peaks at 530, 528.4, and 527.2 eV, which corresponds to the Ti-O, C=O, and lattice oxygen functional groups, respectively [13,14]. To analyze the surface morphology and structural features of a-TiO₂, electron microscopy imaging techniques such as field emission scanning electron microscopy (FE-SEM) and high-resolution transition electron microscopy (HR-TEM) have been used. Fig. 1d and e depict the images of a-TiO₂ at two different magnifications, where we can clearly see the non-uniformly distributed agglomerated particles. The particles are in a few nano to micrometer scales that were further confirmed from TEM analysis, as shown in Fig. 1f, g & h. From HR-TEM images, the lattice fringe width or d -spacing has been determined as 0.28 nm, which belongs to the (101) plane (Fig. 1i). The selected area electron diffraction (SAED) pattern shown in Fig. 1j also reveals the high polycrystallinity of the as-synthesized a-TiO₂. The d -spacing values and crystallographic planes identified from the SAED pattern closely correlate with the results obtained from the XRD analysis. The energy dispersive X-ray analysis (EDAX) depicts the uniform distribution of Ti and O in the sample (Fig. 1k). Therefore, the formation of a-TiO₂, its crystallinity, structural features, and morphology have been confirmed through analytical techniques such as XRD, XPS, FE-SEM, HR-TEM, and EDAX.

3.1. Half-cell performance

The Li⁺ ions de/insertion performance of Li/a-TiO₂ half-cell

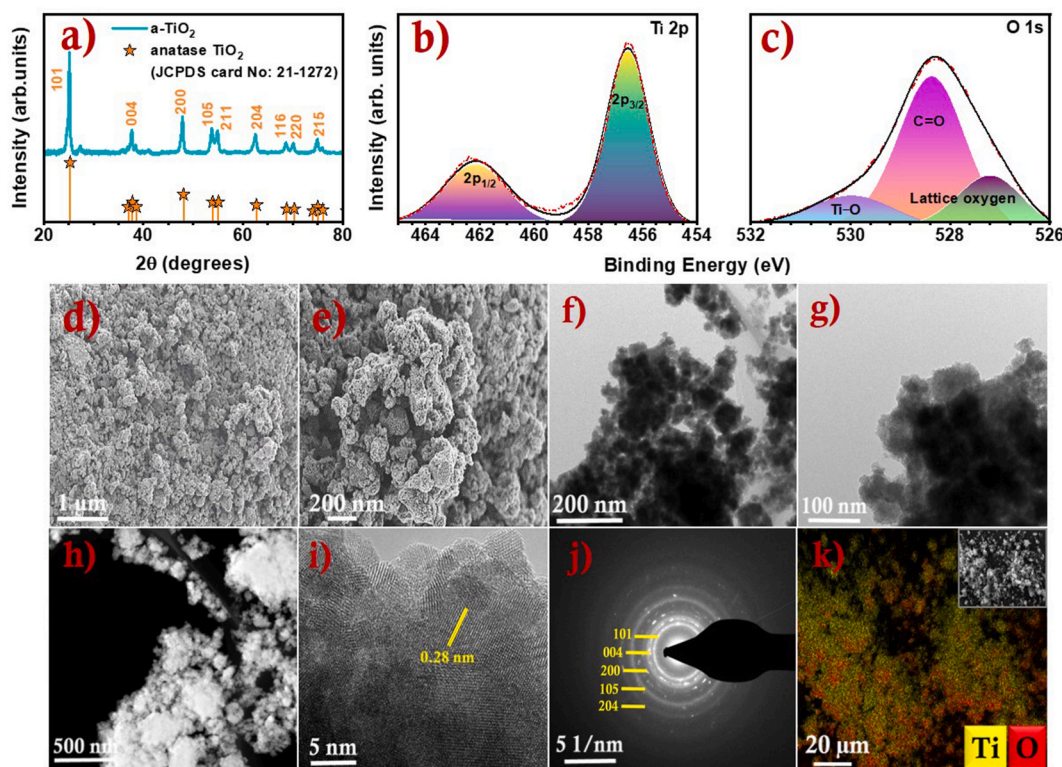
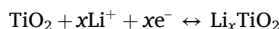


Fig. 1. The physical characterization of a-TiO₂: (a) The XRD pattern, the deconvoluted XPS spectra showing the elements present, (b) Ti 2p, (c) O 1s, (d & e) SEM images at different magnification, (f, g, h, & i) TEM and HR-TEM images showing lattice fringes, (j) SAED pattern, and (k) elemental mapping showing the presence of titanium and oxygen.

assembly was evaluated in a potential window of 1–3 V vs. Li under ambient conditions through both potentiostatic and galvanostatic measurements. The cyclic voltammetry (CV) studies of the cell are performed at different scan rates from 0.1 to 1 mV s⁻¹, as shown in Fig. 2a. The cell exhibited peaks at ~2.1 and ~1.6 V vs. Li during anodic and cathodic scans related to the oxidation and reduction of Ti³⁺/Ti⁴⁺ redox couple. As the scan rate increases, the peak shifts and the broadening of peaks are observed because the peak current is directly proportional to the square root of the scan rate. The well-defined redox peaks correspond to the insertion and extraction of lithium ions in a-TiO₂ as per the following reaction mechanism:



Notably, the prominent flat plateau around ~1.9 and ~1.7 V vs. Li corresponds to the bi-phase reaction mechanism of TiO₂. Generally, in the anatase phase of TiO₂, Li-insertion induces a phase transition from tetragonal (*I*4₁/*amd*) to orthorhombic (Li_{0.5}TiO₂, space group *Pnm*2₁), which is due to the symmetry loss in the *y* direction. This phase transition occurs simultaneously with a spontaneous phase separation of Lithium-poor Li_{0.01}TiO₂ to lithium-rich Li_{0.5}TiO₂ phase [15–17]. The diffusion coefficient of lithium ions for a-TiO₂ was calculated using the following Randles–Sevcicks equation [9] from CV signatures at different scan rates from 0.1 to 1 mV s⁻¹.

$$i_p = 2.69 \times 10^5 n^3/2 C_0 A D^{1/2} \nu^{1/2}$$

where i_p is the peak current, n is the number of Li⁺ ions involved in the electrochemical reaction, C_0 is the Li⁺ ions concentration, A is the cross-sectional area of the electrode, D is the diffusion coefficient of the Li⁺ ions, and ν is the scan rate. A graph is plotted with the peak current vs.

square root of the scan rate for both oxidation and reduction, as depicted in Fig. 2b.

The diffusion coefficient is calculated using the slope ($i_p/\nu^{1/2}$) by substituting the respective values in the above equation. The observed magnitude of the anodic and cathodic diffusion coefficient was $\sim 1.88 \times 10^{-10}$ and $\sim 1.9 \times 10^{-10}$ cm² s⁻¹, respectively. Exnar et al. [18] reported a lithium-ion diffusion coefficient of 1.81×10^{-13} cm² s⁻¹ for anatase TiO₂, while Yan et al. [3] and Aravindan et al. [4] reported values of 1.7×10^{-11} cm² s⁻¹ and 1×10^{-17} cm² s⁻¹, respectively. These values are considerably lower than those obtained in our study, underscoring the enhanced lithium-ion transport properties of our material.

The galvanostatic rate performance of the cell was evaluated from lower to higher current densities (Fig. 2c and d). The reversibility and structural stability were confirmed as the cell retained its initial capacity at the lower current density even after cycling at a high current density of 1.5 A g⁻¹ with a capacity retention of >95 %. The electrochemical cycling performance of a-TiO₂ is analyzed in a potential window of 1–3 V vs. Li at a current density of 0.05 A g⁻¹. The Li/a-TiO₂ half-cell exhibited an initial discharge and charge capacity of 209 and 181 mAh g⁻¹, respectively, at a current density of 0.05 A g⁻¹. An irreversible capacity of ~28 mAh g⁻¹ is common in the case of anatase TiO₂ [10]. The long-term cycling profile in Fig. 2e shows excellent cycling stability with a coulombic efficiency of >99 % after 170 cycles. Fig. 2f illustrates the galvanostatic charge-discharge curves for the 1st, 50th, 100th, and 150th cycles. The flat, distinct plateau around ~1.7 and ~1.9 V vs. Li during the discharging and charging process is analogous to the two-phase reaction mechanism and is correlated with the peak potential noted from CV curves [8,10]. Fig. 2g shows the charge-discharge cycling profile of commercial anatase TiO₂ exhibiting an initial discharge

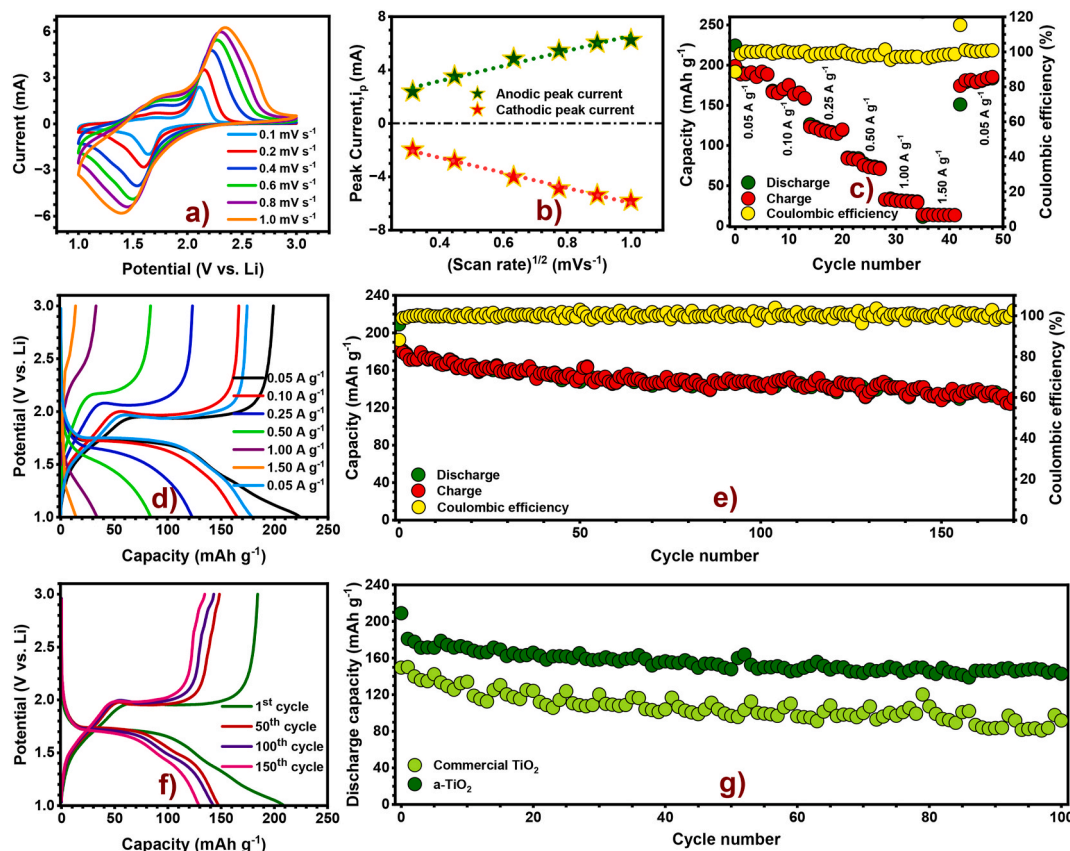


Fig. 2. Electrochemical characterization of a-TiO₂: (a) the CV traces at different scan rates, (b) diffusion coefficient plot, (c) rate performance at different current densities, (d) charge-discharge curves for rate performance at different current densities, (e) cycling stability profile over 170 cycles at a current density of 0.05 A g⁻¹, (f) charge-discharge curves for 1st, 50th, 100th, and 150th cycle in a potential window of 1–3 V vs. Li, (g) cycling stability profile showing the discharge capacity of commercial TiO₂ & a-TiO₂ over 100 cycles at a current density of 0.05 A g⁻¹.

capacity of 149 mAh g^{-1} and a capacity retention of 61% after 100 cycles, which is much lower than the results observed for Li/a-TiO₂. This result clearly distinguishes the electrochemical performance of our LTO-leached a-TiO₂ and commercial TiO₂. An *in-situ* electrochemical impedance spectroscopy (*in-situ* EIS) was recorded to study the mechanism involved in the electrode-electrolyte interface and charge transfer

reaction over a frequency region from 10 kHz to 1 Hz. The EIS was continuously recorded at different potentials to identify the changes in the resistance during the charging and discharging process up to 100 cycles. Fig. 3 represents the corresponding Nyquist plot for the 1st, 5th, 10th, and 100th discharge and charge cycles. The R_{CT} values are observed to be slightly higher for the initial charge-discharge cycles, which are

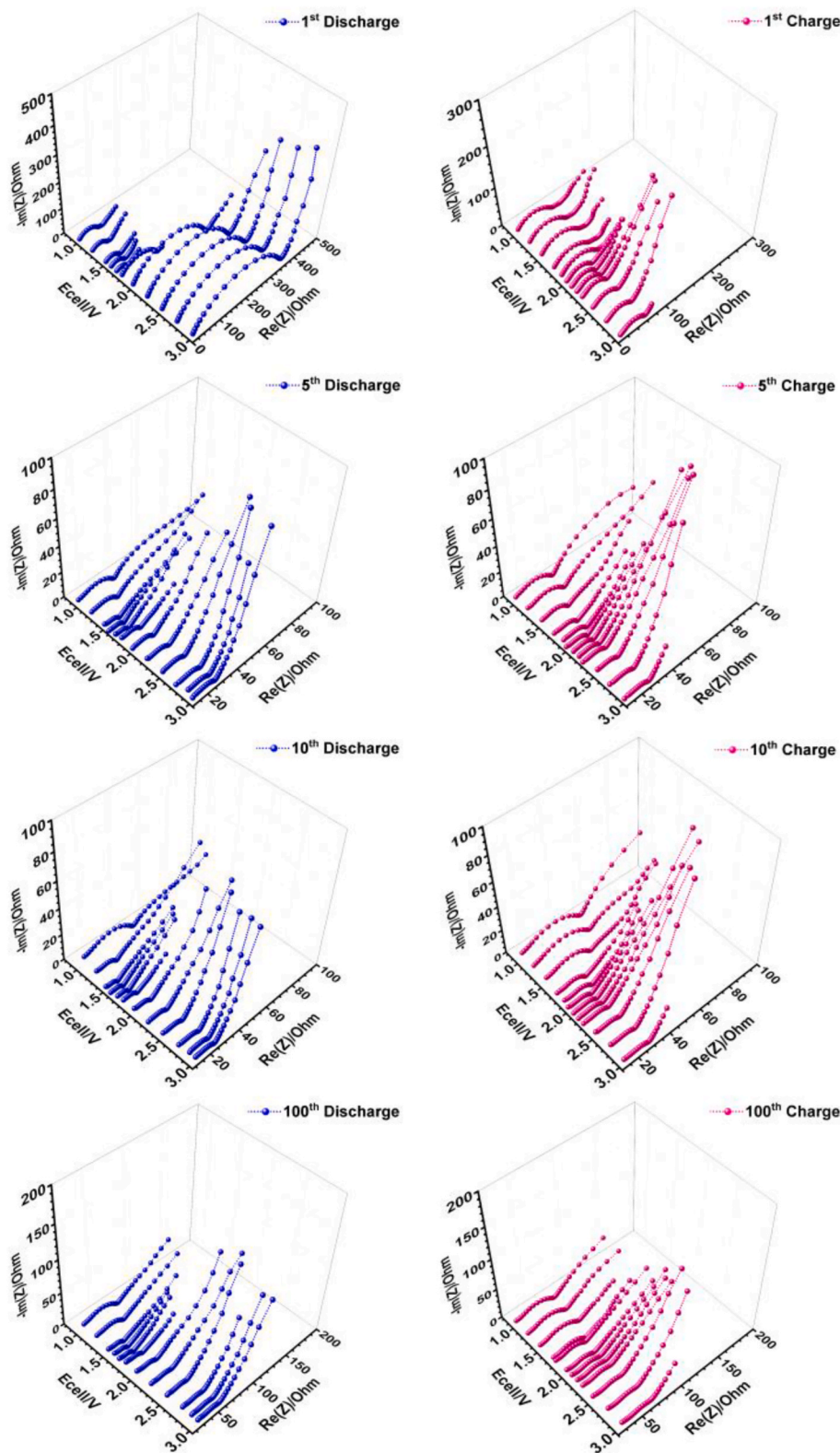


Fig. 3. *in-situ* EIS profile of Li/a-TiO₂ cell with Nyquist plot of 1st, 5th, 10th, & 100th charge-discharge cycles at different potentials.

known, and further, as the cycle progresses, the R_{CT} values are low and stable for more than 100 cycles, indicating the stability of the material.

Fig. S1 represents the electrochemical performance studies of $\text{LiNi}_{0.5}\text{Mn}_{1.5}\text{O}_4$ (LNMO) vs. lithium as a reference or counter electrode in a potential window of 3.5–5 V vs. Li. The CV traces were recorded at different scan rates of 0.1, 0.2, 0.4, 0.6, and 1 mV s^{-1} , as shown in Figure S1 a. The anodic peak at ~ 4.8 V vs. Li corresponds to the oxidation of Ni^{2+} to Ni^{4+} , and the corresponding cathodic peak of reduction is observed at ~ 4.5 V vs. Li [1,15,19,20]. A shoulder peak at 4 V vs. Li is evident at higher scan rates, which suggests the presence of a trace amount of Mn^{3+} . Figures S1 b & c show the rate performance of the Li/LNMO half-cell at various current densities from 0.05 to 1 A g^{-1} . The cell performed well at lower current densities but poorly at higher ones. However, the cell retained its initial capacity at a lower current density even after cycling at a higher current density with $>99\%$ capacity retention. The galvanostatic charge-discharge cycling was conducted at a current density of 0.05 A g^{-1} , as presented in Figures S1 d & e. The significant plateau at about 4.7 V vs. Li corresponds to the $\text{Ni}^{2+}/\text{Ni}^{4+}$ redox pair and is comparable to the peaks seen in CV. The cell rendered a stable performance over 100 cycles with an initial discharge capacity of 131 mAh g^{-1} and a coulombic efficiency of 98 %. The electrochemical performance of activated carbon (AC) was tested in a potential window of 3–4.5 V vs. Li at a current density of 0.1 A g^{-1} . The Li/AC half cell exhibited an initial reversible capacity of 54 mAh g^{-1} and a very stable performance over 500 cycles, as shown in Fig. S2.

Post-modem XRD analysis of the a- TiO_2 electrode is performed after the 100 cycles and illustrated in Fig. 4a. The only additional peaks

observed in the post-cycling XRD are attributed to the Li-poor TiO_2 (Li_xTiO_2), stainless steel (SS) mesh and the binder, TAB-2. No other significant peak shifts or broadening were observed, indicating that the crystallinity and structure of a- TiO_2 remained unchanged. The TEM images of a- TiO_2 after cycling are shown in Fig. 4b–d, and a d -spacing of 0.34 nm was measured. Apparently, the a- TiO_2 particles are embedded into the carbonaceous matrix.

3.2. Full-cell performance

Before the assembly of the full cell, it is necessary to balance the mass of the electrodes. Mass loading of the electrodes was tuned, and the anode-to-cathode ratio was adjusted based on galvanostatic charge-discharge measurements conducted at the same current density. The electrochemical performance of the lithium-ion battery (LIB), fabricated with LNMO as the cathode and a- TiO_2 as the anode, was evaluated in a voltage window of 1.9–3.4 V. The anode: cathode mass ratio was set to be 1:1.4. Fig. 5a illustrates the rate performance of the LNMO/a- TiO_2 at different current rates and could sustain higher current rates with a coulombic efficiency of $>99\%$. The adaptability of the fabricated LIB at various temperatures was analyzed at both low and high temperatures (-10 , 0, 10, 25, & 50 $^{\circ}\text{C}$). The CV trace representing the electrochemical behavior and charge storage mechanism of the fabricated LIB at a scan rate of 0.1 mV s^{-1} is shown in Fig. S3. The specific capacities displayed by the LNMO/a- TiO_2 LIB at different temperatures are shown in Fig. 5b. It is observed that the capacities keep on fading as the temperature increases, which is very obvious due to the electrolyte freezing. The full

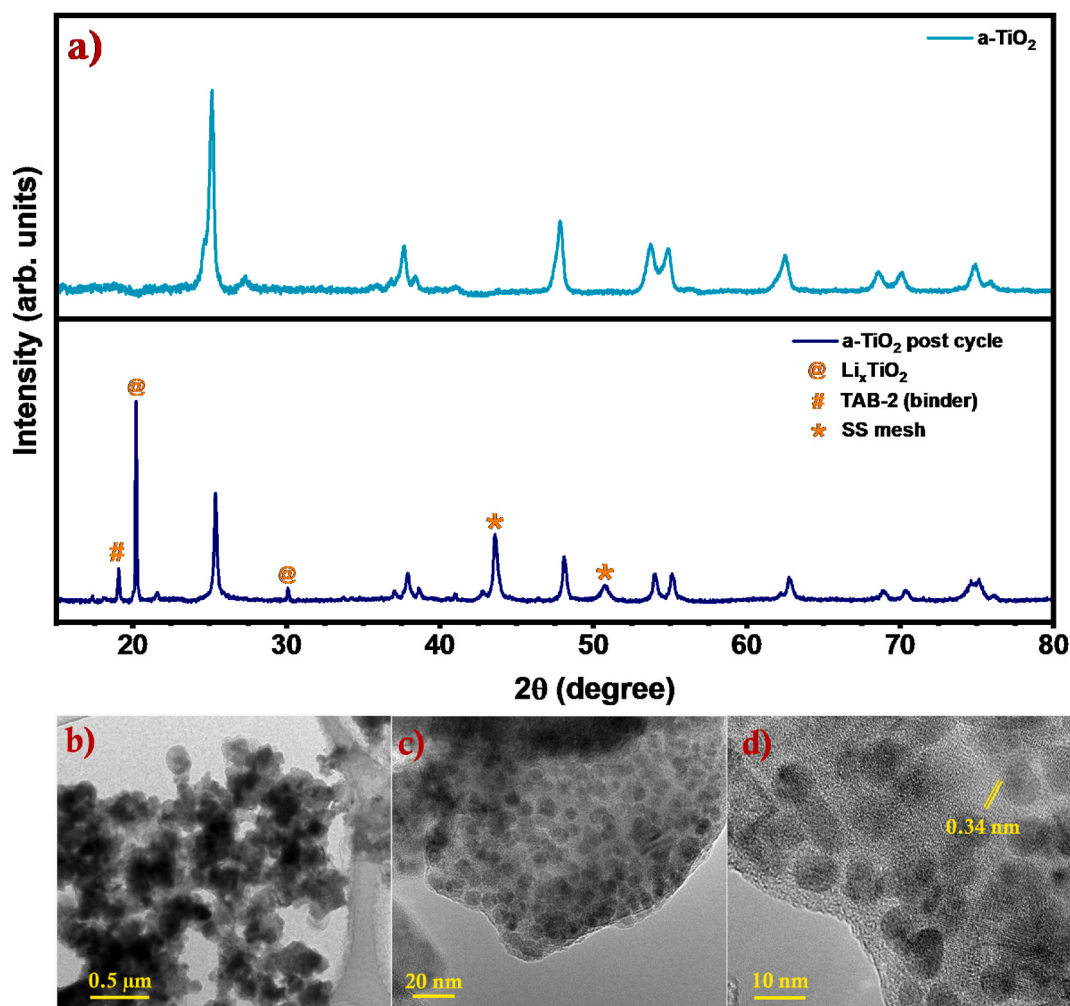


Fig. 4. (a) The XRD pattern of a- TiO_2 before and after charge-discharge cycling, and (b–d) TEM images of post-cycled a- TiO_2 .

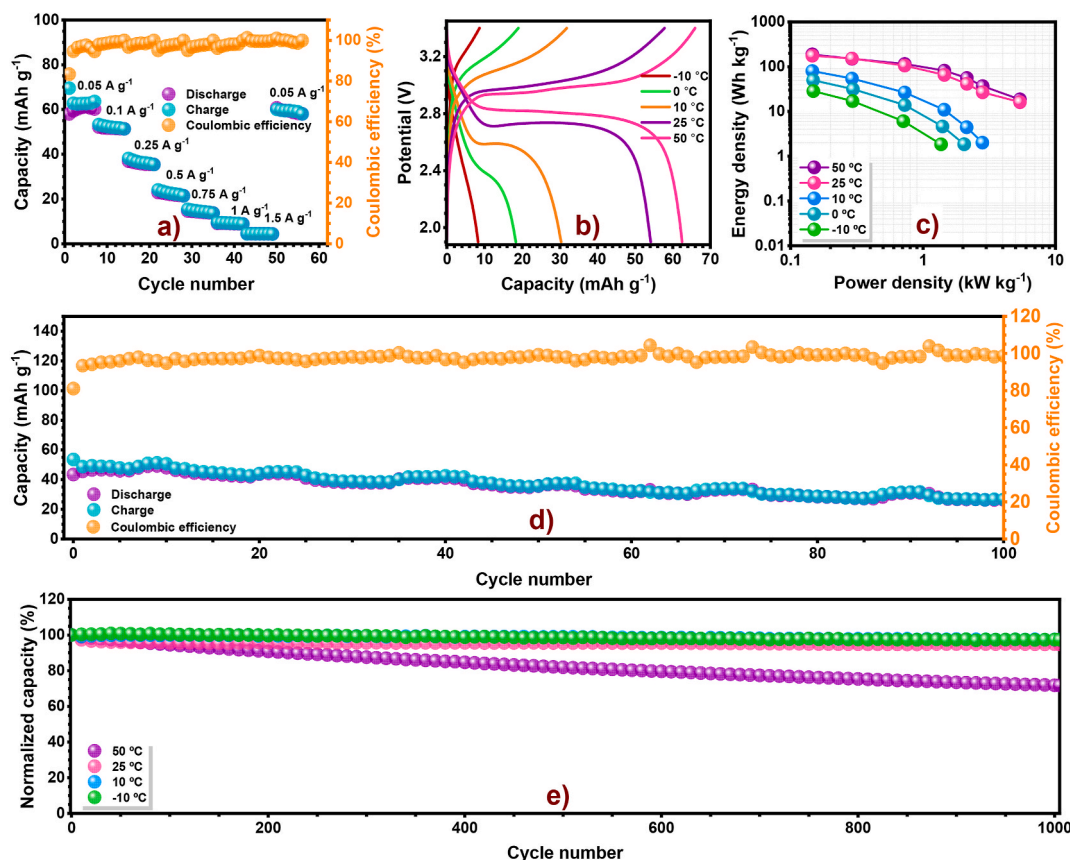


Fig. 5. The electrochemical studies of LNMO/a-TiO₂ LIB: (a) rate performance at different current densities with coulombic efficiency, (b) the charge-discharge curves at different temperatures at a current density of 0.05 A g⁻¹, (c) Ragone plot showing the energy and power density values at different current densities and temperatures, (d) cycling stability profile at a current density of 0.05 A g⁻¹ over 100 cycles, and (e) discharge capacity retention at a current density of 1 A g⁻¹ at different temperatures over 1000 cycles.

cell exhibited a capacity of ~ 50 mAh g⁻¹ (Fig. 5d) at a current density of 0.05 A g⁻¹ based on the total active mass of the anode and cathode with an average voltage of 2.9 V and fairly stable cycling over 100 cycles.

The LIB exhibited a stable cycling profile at a current density of 1 A g⁻¹ for more than 1000 cycles except 50 °C (Fig. 5e). This capacity fading is due to the increased activity of the side reaction at 50 °C. The energy and power density values of the LIB at different current densities and temperature was calculated based on the total mass of the active material of both anode and cathode and obtained a maximum energy and power density of 188 Wh kg⁻¹ and 5.4 kW kg⁻¹, respectively (Fig. 5c). Exnar et al. [18] first to report a 2 V class LiNi_{0.5}Co_{0.5}O₂/TiO₂ exhibiting a reversible capacity of ~ 46 mAh g⁻¹. The full cell (TiO₂/LiC₆) delivered an energy density of ~ 165 Wh kg⁻¹ as per the work reported by Sundaramurthy et al. [21] A similar full cell assembly LNMO/PVdF-HFP/TiO₂¹⁵ reported with an energy density of ~ 285 Wh kg⁻¹ based on the mass of cathode active material. Kim et al. [22] reported a maximum energy of 42 Wh kg⁻¹ at a specific power of 800 W kg⁻¹ for LiMn₂O₄/TiO₂-rGO configuration. Even after morphological modification of TiO₂, LiFePO₄/TiO₂ MCs@CNTs full cell reported by Liu et al. [23] delivered an energy density of 85.5 Wh kg⁻¹ and 48.5 Wh kg⁻¹ at a power density of 19 W kg⁻¹ and 485 W kg⁻¹, respectively. The LNMO/a-TiO₂ assembly we report herein exhibits much higher energy and power density values than the previously reported works.

Similarly, a lithium-ion capacitor (LIC) was fabricated with a-TiO₂ as the anode and activated carbon (AC) as the cathode. The anode: cathode mass ratio was adjusted to 1:3 based on its capacity with metallic lithium in a half-cell assembly. The AC/a-TiO₂ LIC was subjected to galvanostatic charge-discharge cycles at different current rates and temperatures to analyze the high current applicability and the varied climatic

adaptability of the LIC, respectively. As the LIC is a single configuration of the faradaic (battery type a-TiO₂ anode) and non-faradaic (super capacitive-type AC) components, a bi-phase charge storage mechanism occurs, which is confirmed from the CV trace of the fabricated LIC at a scan rate of 0.1 mV s⁻¹ as shown in Fig. S3. During charging, the Li⁺ ions in the electrolyte solution intercalate into the a-TiO₂ via the reduction of Ti⁴⁺ to Ti³⁺ while the PF₆⁻ anions form a double layer with AC across the electrode/electrolyte interface to maintain the charge balance, and the reverse reaction happens while discharging [9,22,24–26].

The AC/a-TiO₂ LIC was tested at a potential window of 0–3 V. The LIC exhibits battery-type behavior in the lower current densities, while the capacitive component is dominant in higher current densities, which is evident from the Ecell vs. time plot in Fig. 6a–e. The electrochemical performance of the LIC at different current densities and temperature conditions (–10, 0, 10, 25, & 50 °C) are examined at a current density of 1 A g⁻¹, where the cell exhibited a very steady performance with a maximum capacity retention of 96 % after 2000 cycles, as depicted in Fig. 6g. The LIC delivered an energy and power density of 73 Wh kg⁻¹ and 4 kW kg⁻¹, respectively, based on the total mass of the anode and cathode (Fig. 6f). The energy and power density obtained for our system is much higher than that reported so far. Wang et al. [25] fabricated a TiO₂-(B) nanowires/carbon nanotube hybrid capacitor that displayed a maximum energy density of 12.5 Wh kg⁻¹. Kim et al. [22] reported an AC/TiO₂-rGO with an energy density of ~ 50 Wh kg⁻¹. Our group has recently reported a similar AC/TiO₂@RG system exhibiting an energy density of 50 Wh kg⁻¹ at a power density of 352 W kg⁻¹ [9]. A comparison between the energy and power density values of the fabricated LNMO/a-TiO₂ and AC/a-TiO₂ configurations at different current densities at room temperature is shown in Fig. 7. At lower current densities,

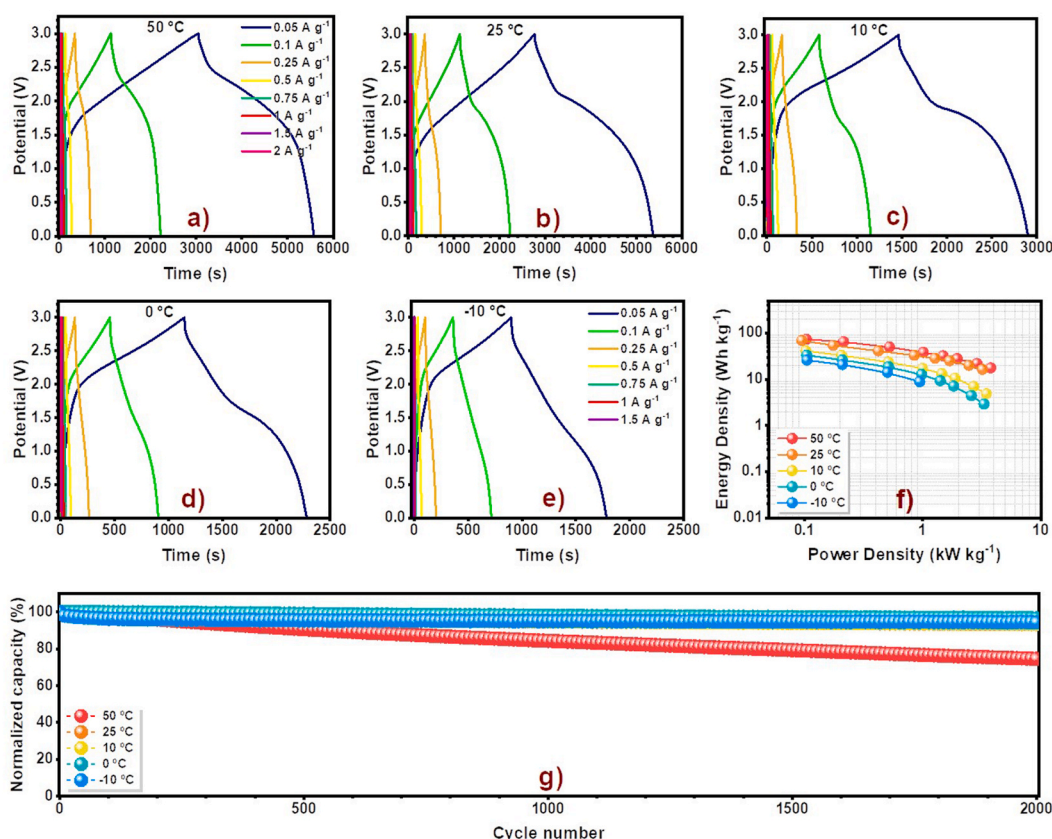


Fig. 6. The electrochemical performance studies of AC/a-TiO₂ LIC: (a–e) charge-discharge curves at different current densities and temperatures, (f) Ragone plot showing the energy and power density values at different temperatures and current densities, and (g) capacity retention at different temperatures at a current density of 1 A g⁻¹ over 2000 cycles.

the LIB exhibited high energy and power densities, but as the current densities increased, a sudden decrease in the performance was observed. The LIC showed fairly stable performance in both high and low current densities, which may be due to the dual charge storage mechanism.

4. Conclusion

In this work, we have successfully demonstrated the reverse

synthesis of anatase phase TiO₂ (a-TiO₂) via leaching it from commercial lithium titanate (Li₄Ti₅O₁₂, LTO). Analytical tools like XRD, XPS, and EDS were adopted to confirm the formation of a-TiO₂. Various other techniques are also employed to study the structural and morphological features of the synthesized a-TiO₂. Then, this a-TiO₂ as the anode, LiNi_{0.5}Mn_{1.5}O₄ (LNMO), and Activated carbon (AC) as the cathode were used for the fabrication of LIB and LIC, respectively. The LNMO/a-TiO₂ cell delivered a maximum energy density of 188 Wh kg⁻¹ and a power density of 5.4 kW kg⁻¹ with a stable cycling performance over 1000 cycles at different temperatures. The fabricated AC/a-TiO₂ LIC exhibited an energy and power density of 73 Wh kg⁻¹ and 4 kW kg⁻¹, respectively, based on the total active material mass of the anode and cathode. In addition, the LIC rendered a very good cyclability with a maximum capacity retention of 96% over 2000 cycles and promising performance at various temperatures (-10, 0, 10, 25, & 50 °C). This new, low-cost, scalable, and eco-friendly synthesis of a-TiO₂ paved the way for developing efficient energy storage devices by re-utilization of LTO-based LIBs that are abandoned from stationary applications and electric vehicles.

CRedit authorship contribution statement

Shaji Jyothilakshmi: Conceptualization, Methodology, Investigation, Data curation, Writing – original draft, Validation, Funding acquisition, Formal analysis. **Yun-Sung Lee:** Writing – review & editing, Project administration, Funding acquisition, Formal analysis, Conceptualization. **Vanchiappan Aravindan:** Writing – review & editing, Writing – original draft, Validation, Supervision, Project administration, Funding acquisition, Formal analysis, Conceptualization.

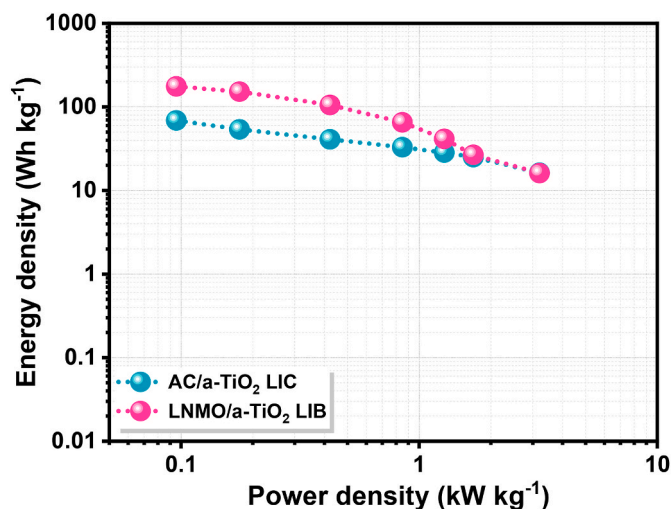


Fig. 7. Ragone plot depicting the comparison between the energy density and power density values of the fabricated LIB and LIC at different current densities at room temperature.

Declaration of competing interest

The authors declare that they have no known competing financial interests or personal relationships that could have appeared to influence the work reported in this paper.

Acknowledgements

SJ thanks the Prime Minister's Research Fellowship (0902009) for financial support. YSL acknowledges the financial support from the National Research Foundation of Korea (NRF) grant funded by the Korean government (Ministry of Science, ICT & Future Planning) (No. RS-2023-00208361). VA acknowledges financial support from the Anusandhan National Research Foundation through Swarnajayanti Fellowship (SB/SJF/2020-21/12).

Appendix A. Supplementary data

Supplementary data to this article can be found online at <https://doi.org/10.1016/j.jpowsour.2025.237543>.

Data availability

Data will be made available on request.

References

- [1] P. Suresh Kumar, V. Aravindan, J. Sundaramurthy, V. Thavasi, S.G. Mhaikalkar, S. Ramakrishna, S. Madhavi, High performance lithium-ion cells using one dimensional electrospun TiO₂ nanofibers with spinel cathode, *RSC Adv.* 2 (21) (2012) 7983–7987, <https://doi.org/10.1039/c2ra20645e>.
- [2] M. Madian, A. Eychemüller, L. Giebeler, Current advances in TiO₂-Based nanostructure electrodes for high performance lithium ion batteries, *Batteries* 4 (1) (2018), <https://doi.org/10.3390/batteries4010007>.
- [3] X. Yan, Z. Wang, M. He, Z. Hou, T. Xia, G. Liu, X. Chen, TiO₂ nanomaterials as anode materials for lithium-ion rechargeable batteries, *Energy Technol.* 3 (8) (2015) 801–814, <https://doi.org/10.1002/ente.201500039>.
- [4] V. Aravindan, Y.S. Lee, R. Yazami, S. Madhavi, TiO₂ polymorphs in 'Rocking-Chair' Li-Ion batteries, *Mater. Today* 18 (6) (2015) 345–351, <https://doi.org/10.1016/j.MATOD.2015.02.015>.
- [5] S. Liang, X. Wang, Y.J. Cheng, Y. Xia, P. Müller-Buschbaum, Anatase titanium dioxide as rechargeable ion battery electrode - a chronological review, *Energy Storage Mater.* 45 (October 2021) (2022) 201–264, <https://doi.org/10.1016/j.ensm.2021.11.023>.
- [6] B. Zachau-Christiansen, K. West, T. Jacobsen, S. Atlung, Lithium insertion in different TiO₂ modifications, *Solid State Ionics* 28–30 (PART 2) (1988) 1176–1182, [https://doi.org/10.1016/0167-2738\(88\)90352-9](https://doi.org/10.1016/0167-2738(88)90352-9).
- [7] Z. Liu, Y.G. Andreev, A. Robert Armstrong, S. Brutti, Y. Ren, P.G. Bruce, Nanostructured TiO₂(B): the effect of size and shape on anode properties for Li-Ion batteries, *Prog. Nat. Sci. Mater. Int.* 23 (3) (2013) 235–244, <https://doi.org/10.1016/j.pnsc.2013.05.001>.
- [8] D.P. Opra, S.V. Gnedenkova, S.L. Sinebryukhov, Recent efforts in design of TiO₂(B) anodes for high-rate lithium-ion batteries: a review, *J. Power Sources* 442 (2019) 227225, <https://doi.org/10.1016/j.jpowsour.2019.227225>.
- [9] S. Jyothilakshmi, P. Meshram, Abhilash, Y.-S. Lee, V. Aravindan, Graphite from dead Li-Ion batteries: a "Powerful" additive for fabrication of high-performance Li-Ion capacitors, *Adv. Mater. Technol.* 9 (7) (2024) 2301000, <https://doi.org/10.1002/admt.202301000>.
- [10] J. Sundaramurthy, V. Aravindan, P.S. Kumar, S. Madhavi, S. Ramakrishna, Electrospun TiO_{2-x} nanofibers as insertion anode for Li-ion battery applications, *J. Phys. Chem. C* 118 (30) (2014) 16776–16781, <https://doi.org/10.1021/jp412787z>.
- [11] A.O. Bokuninaeva, A.S. Vorokh, Estimation of particle size using the debye equation and the scherrer formula for polyphasic TiO₂ powder, *J. Phys. Conf. Ser.* 1410 (1) (2019) 12057, <https://doi.org/10.1088/1742-6596/1410/1/012057>.
- [12] S. Haukka, E.L. Lakomaa, O. Jylha, J. Vilhunen, S. Hornytzkij, Dispersion and distribution of titanium species bound to silica from titanium tetrachloride, *Langmuir* 9 (12) (1993) 3497–3506, <https://doi.org/10.1021/la00036a026>.
- [13] A. Crake, K.C. Christoforidis, A. Gregg, B. Moss, A. Kafizas, C. Petit, The effect of materials architecture in TiO₂/MOF composites on CO₂ photoreduction and charge transfer, *Small* 15 (11) (2019) 1805473, <https://doi.org/10.1002/sml.201805473>.
- [14] F. Lange, H. Schmelz, H. Knözinger, An X-Ray photoelectron spectroscopy study of oxides of arsenic supported on TiO₂, *J. Electron. Spectrosc. Relat. Phenom.* 57 (3) (1991) 307–315, [https://doi.org/10.1016/0368-2048\(91\)80017-O](https://doi.org/10.1016/0368-2048(91)80017-O).
- [15] N. Arun, V. Aravindan, S. Jayaraman, N. Shubha, W.C. Ling, S. Ramakrishna, S. Madhavi, Exceptional performance of a high voltage spinel LiNi_{0.5}Mn_{1.5}O₄ cathode in all one dimensional architectures with an anatase TiO₂ anode by electrospinning, *Nanoscale* 6 (15) (2014) 8926–8934, <https://doi.org/10.1039/c4nr01892c>.
- [16] L. Kavan, Electrochemistry of titanium dioxide: some aspects and highlights, *Chem. Rec.* 12 (1) (2012) 131–142, <https://doi.org/10.1002/tcr.201100012>.
- [17] Z. Yang, D. Choi, S. Kerisit, K.M. Rosso, D. Wang, J. Zhang, G. Graff, J. Liu, Nanostructures and lithium electrochemical reactivity of lithium titanates and titanium oxides: a review, *J. Power Sources* 192 (2) (2009) 588–598, <https://doi.org/10.1016/j.jpowsour.2009.02.038>.
- [18] I. Exnar, L. Kavan, S.Y. Huang, M. Grätzel, Novel 2 V rocking-chair lithium battery based on nano-crystalline titanium dioxide, *J. Power Sources* 68 (2) (1997) 720–722, [https://doi.org/10.1016/S0378-7753\(96\)02581-5](https://doi.org/10.1016/S0378-7753(96)02581-5).
- [19] L. Wang, H. Li, X. Huang, E. Baudrin, A comparative study of Fe₃O₄ and P₄O₃₂ "LiNi_{0.5}Mn_{1.5}O₄", *Solid State Ionics* 193 (1) (2011) 32–38, <https://doi.org/10.1016/j.ssi.2011.04.007>.
- [20] K. Takahashi, M. Saitoh, M. Sano, M. Fujita, K. Kifune, Electrochemical and structural properties of a 4.7 V-Class LiNi_{0.5}Mn_{1.5}O₄ positive electrode material prepared with a self-reaction method, *J. Electrochem. Soc.* 151 (1) (2003) A173, <https://doi.org/10.1149/1.1633267>.
- [21] S. Jayaraman, V. Aravindan, N. Shubha, M. Ulaganathan, S. Madhavi, Exploring anatase TiO₂ nanofibers as new cathode for constructing 1.6 V class "Rocking-Chair" type Li-Ion cells, Part. \& Part. Syst. Charact. 33 (6) (2016) 306–310, <https://doi.org/10.1002/ppsc.201600044>.
- [22] H.K. Kim, D. Mhamane, M.S. Kim, H.K. Roh, V. Aravindan, S. Madhavi, K.C. Roh, K.B. Kim, TiO₂-Reduced graphene oxide nanocomposites by microwave-assisted forced hydrolysis as excellent insertion anode for Li-Ion battery and capacitor, *J. Power Sources* 327 (2016) 171–177, <https://doi.org/10.1016/j.jpowsour.2016.07.053>.
- [23] X. Liu, L. Zhao, S. Wang, M. Chao, Y. Li, J. Leng, J. Zhang, Z. Tang, Hierarchical-structure anatase TiO₂ with conductive network for high-rate and high-loading lithium-ion battery, *Sci. Bull.* 64 (16) (2019) 1148–1151, <https://doi.org/10.1016/j.scib.2019.06.022>.
- [24] H. Kim, M.-Y. Cho, M.-H. Kim, K.-Y. Park, H. Gwon, Y. Lee, K.C. Roh, K. Kang, A novel high-energy hybrid supercapacitor with an anatase TiO₂-Reduced graphene oxide anode and an activated carbon cathode, *Adv. Energy Mater.* 3 (11) (2013) 1500–1506, <https://doi.org/10.1002/aenm.201300467>.
- [25] Q. Wang, Z.H. Wen, J.H. Li, A hybrid supercapacitor fabricated with a carbon nanotube cathode and a TiO₂-B nanowire anode, *Adv. Funct. Mater.* 16 (16) (2006) 2141–2146, <https://doi.org/10.1002/adfm.200500937>.
- [26] V. Aravindan, N. Shubha, W. Chui Ling, S. Madhavi, Constructing high energy density non-aqueous Li-Ion capacitors using monoclinic TiO₂-B nanorods as insertion host, *J. Mater. Chem. A* 1 (20) (2013) 6145–6151, <https://doi.org/10.1039/c3ta11103b>.